RESEARCH ARTICLE

Effects of micro-sprinkler irrigation arrangement on soil moisture distribution under different soil conditions

HaowenYang[1], Yun Yang[2], Jian Zheng[1, 3, *], Chunxia Wang[2], Hao Song[2]

[1]College of Energy and Power Engineering, Lanzhou University of Technology, Lanzhou, Gansu, China.
[2]Water Conservancy Science Research Institute of Linxia Hui Autonomous Prefecture, Linxia, Gansu, China.
[3]Key Laboratory of Complementary Energy System of Biomass and Solar Energy, Lanzhou, Gansu, China.

Received: September 17, 2025; **accepted:** December 20, 2025.

As a water-scarce nation, China sees a significant proportion of its water resources allocated to agriculture. Micro-sprinkler irrigation systems can significantly improve the efficiency of agricultural irrigation water use. The design layout of these systems plays a crucial role in determining the uniformity of water distribution and soil moisture. To investigate the effect of micro-sprinkler designs on the actual water content distribution and irrigation uniformity under different soil conditions, this study was conducted in three primary crop soils of the Loess Plateau in Linxia Hui and Tibetan Autonomous Prefecture, Gansu, China. The soil water characteristic curves and permeability parameters were determined, and a micro-irrigation system was installed. Based on the water distribution results, a micro-irrigation system suitable for each soil type was proposed. The results showed that yellow loam had the best water holding property among the three soils, while yellow loess had the best water effectiveness. The vertical transport speed of the wetting front of yellow loam was the slowest, and the cumulative amount of infiltration was the largest. In yellow loam, the best irrigation uniformity could be obtained by the square-triangle arrangement, while in black clay loam soil and yellow sandy loam, the best irrigation uniformity could be obtained by the square arrangement. This research provided technical guidance for the standardized construction of micro-sprinkler irrigation systems and offered a theoretical basis for enhancing the design of efficient water-saving irrigation systems in protected agriculture.

Keywords: micro-sprinkler irrigation; soil water characteristic curve; soil water retention performance; water distribution; homogeneity factor.

[*]**Corresponding author:** Jian Zheng, College of Energy and Power Engineering, Lanzhou University of Technology, Lanzhou, Gansu 730050, China. Email: pojianilb645@163.com.

Introduction

As a water-scarce nation, China sees a significant proportion of its water resources allocated to agriculture. Micro-sprinkler irrigation systems can effectively enhance the efficiency of agricultural irrigation water use. The layout of these systems directly influences the uniformity of water distribution and soil moisture distribution. Micro-sprinkler irrigation is an efficient irrigation technology characterized by small droplet size and high atomization, which not only increases soil moisture but also enables rapid cooling and humidification, helping to regulate the local microclimate and making it suitable for precision irrigation [1]. The uniformity of water distribution in micro-sprinkler irrigation directly affects soil moisture content, which, in turn, plays a vital role in helping plants grow and the formation of yield

quality [2]. However, in practical applications, there is often a significant discrepancy between the theoretical irrigation uniformity of the system and the actual moisture infiltration into the soil. This is largely influenced by the soil's moisture infiltration characteristics [3]. Different soil types exhibit notable differences in moisture infiltration characteristics due to variations in the texture and structure of the soil [4, 5]. Despite this, research on the relationship between soil moisture infiltration characteristics and micro-sprinkler irrigation uniformity remains limited.

Research on the distribution of water volume in micro-sprinkler irrigation has predominantly focused on factors such as wind and slope that cannot be controlled. Studies examining the effects of nozzle configuration and operating pressure on irrigation uniformity often employ numerical models. These calculations typically use the water distribution from a single nozzle and apply the principle of superposition to derive the uniformity of irrigation from various nozzle combinations and spacing [6]. However, there is a lack of experimental studies investigating how differences in commonly used layout arrangements such as square, equilateral triangle, and rectangular configurations under varying soil conditions affect the actual moisture distribution of the soil and irrigation uniformity in micro-sprinkler systems.

This study first determined the soil moisture characteristic curves of three main soil types in the Loess Plateau located in the Linxia Hui and Tibetan Autonomous Prefecture of Gansu, China including yellow clay, yellow loess, and black loess under varying bulk densities. This step was taken to elucidate the variation patterns of water retention capacity across different soil types. The vertical soil column experiments were then conducted to obtain infiltration characteristic parameters for different soils, establishing the connection between the vertical movement distance of the wetting front and cumulative infiltration over time. Three micro-sprinkler irrigation layout arrangements were eventually set up to analyze the distribution of soil moisture content, and suitable micro-sprinkler configurations under different soil conditions were proposed using the coefficient of uniformity of soil moisture (CUs) and the distribution uniformity of soil moisture (DUs) [7]. The results of this research would provide technical guidance for the standardized construction of micro-sprinkler irrigation systems and offer a theoretical basis for enhancing the design of efficient water-saving irrigation systems in protected agriculture.

Materials and methods

Soil sample collection

The soil samples used for testing were all collected from Linxia County, Linxia Prefecture, Gansu, China at a depth of 0 - 40 cm. After collection, the soils were air-dried, and visible root remnants and leaf materials were eliminated. Subsequently, the soils were subjected to sieving through a 2 mm diameter mesh and were thoroughly homogenized for future applications. A Mastersizer 2000 laser particle size analyzer (Malvern Panalytical, Shanghai, China) was used to determine the mechanical composition of the soils. Three types of soil including yellow loam, black clay loam, and yellow sandy loam with soil bulk densities of 1.30 g/cm^3, 1.35 g/cm^3, and 1.40 g/cm^3 were used in this research. The clay, silt, and sand volumetric percentages were 9.06%, 83.21%, and 7.73% for yellow loam, 8.46%, 81.51%, and 10.03% for black clay loam, and 8.06%, 80.31%, and 11.63% for yellow sandy loam, respectively.

Soil moisture characteristic curve

The soil moisture characteristic curve was determined utilizing the centrifuge method. The test soils were packed into ring knives in layers and then saturated for 24 hours in distilled water. The ring knives were placed in a suspended position until no more gravitational water was discharged, indicating the soil samples had reached saturation. The mass was determined utilizing an electronic balance with an accuracy of 0.01 g. Soil moisture content under varying soil

water suction levels was determined in accordance with the standard procedure for measuring soil moisture characteristic curves using Hitachi CR 21G II high-speed freezing centrifuge (Hitachi, Tokyo, Japan). After the centrifugation, the samples were dried at a constant temperature of 105°C in a controlled thermostatic oven until a consistent weight was achieved. The soil moisture content was then calculated. Each of the three soil types was tested at three soil bulk densities with four repetitions, and the mean value was utilized as the outcome of the experiment. The Van Genuchten model was used to fit the soil moisture characteristic curve [8] as follows, and the model parameters were established through the fitting process utilizing the RETC software (https://retc-ca.com/pvmi).

$$\theta(h) = \begin{cases} \theta_r + \frac{\theta_s - \theta_r}{[1+|\alpha h|^n]^m} & (h < 0) \\ \theta_s & (h > 0) \end{cases} \quad (1)$$

where $\theta(h)$ was the relative moisture content of the soil (cm^3/cm^3). θs was the saturated volumetric moisture content of the soil (cm^3/cm^3). θr was the remaining volumetric water content present in the soil (cm^3/cm^3). α was the reciprocal of the air entry value (/cm). h was the matric potential (cm). n and m were empirical fitting parameters that determined the shape of the characteristic curve, where m = 1 - 1/n.

Soil pores

The dimensions and spatial arrangement of soil pores could be indirectly reflected by the soil moisture characteristic curve. If the soil pores were assumed to be cylindrical capillaries, the correlation between suction and capillary diameter could be succinctly represented as below.

$$s = 4\sigma / d \quad (2)$$

where σ was the surface tension coefficient of water, which was typically taken as 75×10^{-5} N/cm under room temperature. S was the soil water suction, measured in meters (m). d was the equivalent pore diameter, measured in millimeters (mm). By calculating the equivalent pore diameter, the pore size and distribution corresponding to different soil water contents could be determined. An analysis of the alterations in the water retention capacity of soils could be conducted by examining the distribution of pore sizes across various treatment conditions.

Characteristics of soil infiltration

The experimental setup comprised a soil column and a water delivery system. The soil column was constructed from polymethyl methacrylate, featuring a diameter of 7.3 cm and a height of 45 cm. The Mariotte bottle possessed a cross-sectional area of 50 cm^2 and a height of 80 cm. The soil bulk density was 1.35 g/cm^3. During the packing of the soil column, the soil was deposited in stratified layers with each layer being 10 cm thick. The edges were compacted to avoid gaps and prevent edge effects. A layer of filter paper was positioned atop the soil column to mitigate the effects of the infiltrating water and to promote uniformity in the infiltration process. The Mariotte bottle was employed as a mechanism for water supply with the water head regulated at a height of 2 cm. Following the principle of observing closely at first and then at longer intervals, the water stage in the Mariotte bottle, infiltration time, and the migration distance of the wetting front were recorded. When the infiltration time reached 60 minutes, the experiment was concluded, and the accumulated water was drained.

Distribution characteristics of soil moisture content in micro-spray irrigation

The experiment utilized ground-inserted micro-sprinklers with a spray diameter of 30 cm, a flow quantity of 0.8 L/min, and an operating pressure of 0.3 MPa. The height above ground was set to 20 cm, and the bulk density was 1.35 g/cm^3. The arrangement methods employed in the study were square, equilateral triangular, and rectangular layouts (Figure 1A). In the square layout, nozzle spacing (Sr) equaled to branch pipe spacing (Sl) and spray radius (R) as 30 cm, while

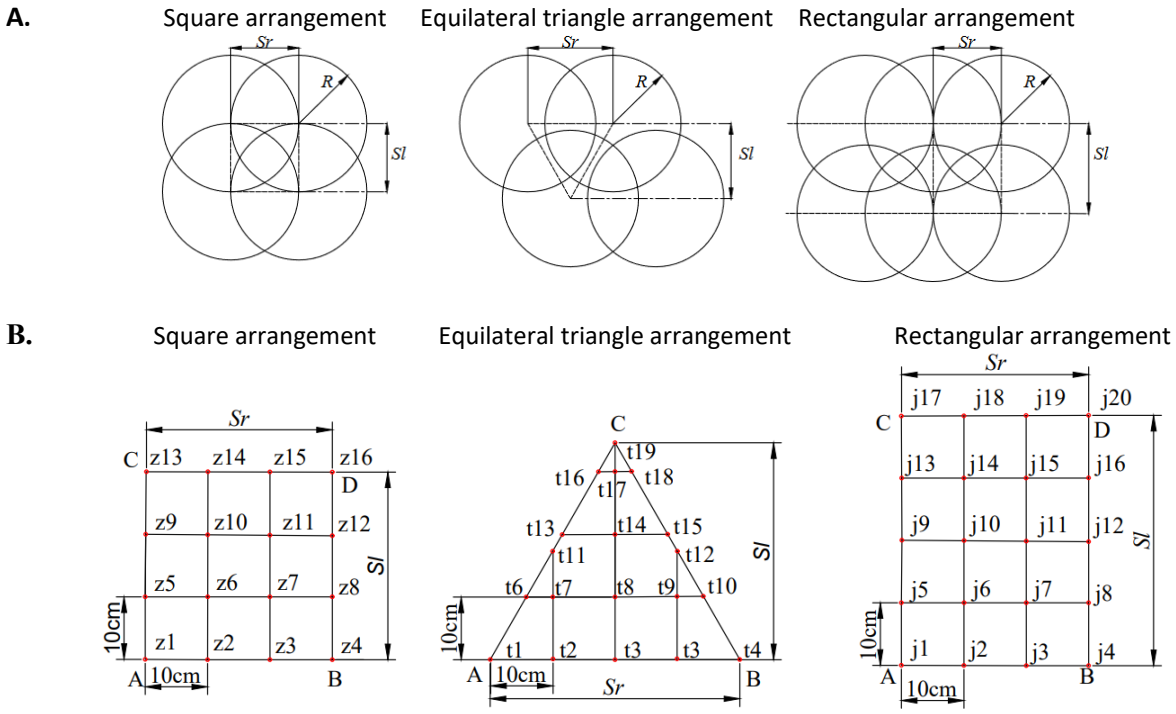

Figure 1. Diagram of sprinkler combination (**A**) and measuring point location (**B**). Sr: nozzle spacing. Sl: branch pipe spacing. R: spray radius.

in the equilateral triangular layout, Sr was 1.33 with R as 40 cm, and Sl was 1.15 with R as 34.64 cm. In the rectangular layout, Sr equaled to R as 30 cm, and Sl was 1.33 with R as 40 cm. This study focused only on the area covered by the sprinkler combinations. Therefore, the locations of the measurement points for each arrangement were shown in Figure 1B. In the square layout, within the area formed by four sprinklers of A, B, C, D, a grid with 10 cm spacing was drawn in the direction of the lateral pipe and the sprinkler direction. The grid nodes served as measurement points with totaling 16 points and were labeled as z1 to z16. In the equilateral triangular layout, within the area formed by three sprinklers of A, B, C, a 10 cm grid was used for measurement points with additional points at the intersections of the grid and the triangular boundary. This arrangement included 19 measurement points, labeled t1 to t19. In the rectangular layout, within the area formed by four sprinklers of A, B, C, D, a grid with 10 cm spacing was similarly used along the lateral pipe and sprinkler direction. There were 20 measurement points in total, labeled j1 to j20. During the experiment, water was supplied from a water tank, and the sprinklers operated at a fixed flow rate for 15 minutes. Thirty minutes after spraying ended, soil surface samples were collected and weighed with a precision of 0.01 g. The samples were then placed in a thermostatic oven for drying at a temperature of 105°C until a constant weight was achieved to determine the moisture content of the soil.

Uniformity of soil moisture distribution

The distribution of soil moisture content was evaluated using the CUs and DUs calculated as follows.

$$CU_s = \left(1 - \frac{\sum_{i=1}^{n} |xi - \bar{x}|}{\sum_{i=1}^{n} x_i}\right) \times 100\% \quad (3)$$

where CU_s was the coefficient of uniformity of soil moisture. *xi* was the gravimetric water content at the i-th measuring point, expressed as a percentage (%). $\bar{x}$ was the mean gravimetric water content calculated from all measurement

locations, expressed as a percentage (%). *n* was the quantity of measurement points.

$$DU_S = \frac{\overline{x'}}{\bar{x}} \times 100\% \quad (4)$$

where DU_s was the distribution uniformity of soil moisture. $\bar{x}$ was the mean gravimetric water content calculated from all measurement locations, expressed as a percentage (%). $\overline{x'}$ was the average gravimetric moisture content of the lowest quartile of the arranged gravimetric water contents of the measurement points, expressed as a percentage (%).

Data Processing

Each treatment was replicated four times, and the mean value was utilized as the experimental outcome. Graphs were created using Origin Pro 2022 (https://www.originlab.com/) and Surfer software (https://surfer-grapher.com/surfer/), while curve fitting was performed using RETC software.

Results

Soil moisture characteristic curve

The soil-water characteristic curve served as a key indicator of soil hydrodynamic properties. The curves for different soils exhibited similar trends. Specifically, when the soil water suction (S) < 1,000 cm, the volumetric water content decreased rapidly with increasing suction, showing minimal differences. After S > 1,000 cm, the curve became relatively flat. There were notable differences in the values of the soil water characteristic curves at varying bulk densities, yet they displayed similar trends. When the soil water suction equaled to 1,000 cm, the volumetric water content of soils with a bulk density of 1.30 g/cm³ was greater than that of soils with bulk densities of 1.35 g/cm³ and 1.40 g/cm³. The lowest moisture content was observed at 1.40 g/cm³, indicating that the capacity for water retention increased as the bulk density decreased among the three soil types. At a volumetric water content of 0.23 cm³/cm³ (70% of field capacity for yellow loam at 1.30 g/cm³), the soil suction at 1.40 g/cm³ was the lowest, while it was the highest at 1.30 g/cm³, which indicated that, at equivalent water content levels, soils exhibiting higher bulk density demonstrated enhanced water availability compared to those with lower bulk density. Furthermore, when considering soils with the same bulk density, notable numerical variations were observed in the soil water characteristic curves across different soil types, despite the overarching trends being largely consistent. The results also showed that, at a soil water suction of 1,000 cm, the soil water content was in the order of yellow loam > black clay loam > yellow sandy loam, indicating that yellow loam had the best water retention capacity, followed by black clay loam, while yellow sandy loam had the least. At a volumetric water content of 0.23 cm³/cm³, the order of water suction was yellow sandy loam < black clay loam < yellow loam, suggesting that the water availability in yellow loam was less favorable than that in black clay loam, while yellow sandy loam had better water availability compared to black clay loam (Figure 2). To further analyze the impact of different bulk densities on the capacity for water retention of the three soils, the Van Genuchten model was employed to analyze and fit the experimental data. The results showed that the correlation coefficients (R^2) values for all the fitted curves were greater than 0.97, indicating that the parameter fit of the Van Genuchten model was satisfactory, and all the parameters could be used to elucidate the patterns of variation of the soil moisture characteristic curves (Table 1). Bulk density conditions had a certain impact on the characteristic parameters of soil water retention capacity. In yellow loam, the residual water content θr at 1.30 g/cm³ and 1.35 g/cm³ bulk densities increased by 64.62% and 43.96%, respectively, compared to that at 1.40 g/cm³ bulk density, and the saturated water content θs increased by 6.83% and 4.28%, respectively. In black clay loam, the residual water content θr at 1.30 g/cm³ and 1.35 g/cm³ bulk densities increased by 61.68% and 43.71%, respectively, compared to that at 1.40 g/cm³, and the

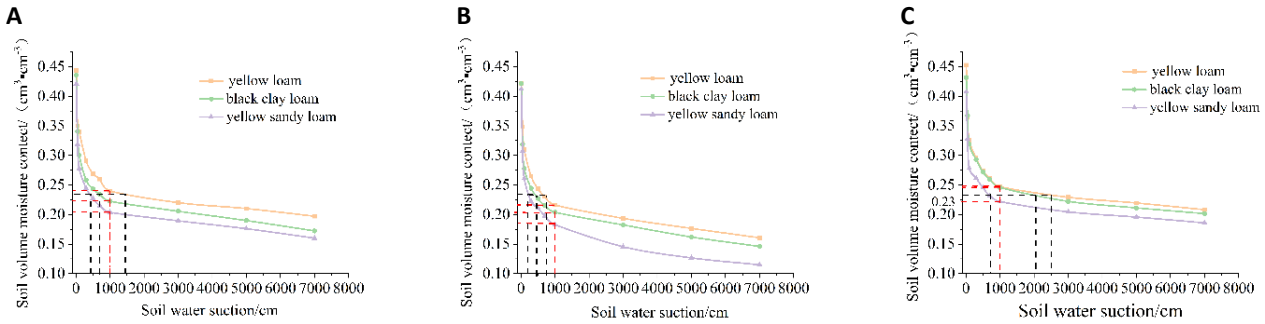

Figure 2. The relationship between soil water characteristics and varying soil bulk density. **A.** bulk density 1.30g/cm^3. **B.** bulk density 1.35g/cm^3. **C.** bulk density 1.40 g/cm^3.

Table 1. Fitting parameters of Van-Genuchten model for soil moisture characteristic curve.

Soil bulk density (g/cm^3)	Soil type	Fitting parameters					R^2
		θr (cm^3/cm^3)	θ_s (cm^3/cm^3)	α	n	m	
1.30	Yellow - hemp soil	0.1771	0.4644	0.0519	1.34785	0.2581	0.9905
	Dark loessial soil	0.1725	0.4476	0.0527	1.2739	0.2150	0.9937
	Loessal soil	0.1639	0.4267	0.0638	1.3641	0.2669	0.9962
1.35	Yellow - hemp soil	0.1549	0.4533	0.0549	1.2629	0.2082	0.9942
	Dark loessial soil	0.1533	0.4451	0.0492	1.3795	0.2751	0.9901
	Loessal soil	0.1457	0.4332	0.0542	1.4031	0.2873	0.9937
1.40	Yellow - hemp soil	0.1076	0.4347	0.0439	1.2721	0.2139	0.9796
	Dark loessial soil	0.1067	0.4339	0.0625	1.3033	0.2327	0.9856
	Loessal soil	0.0868	0.4254	0.0800	1.2291	0.1864	0.9943

saturated water content θs increased by 3.16% and 2.60%, respectively. In yellow sandy loam, the residual water content θr at 1.30 g/cm³ and 1.35 g/cm³ bulk densities increased by 104.88% and 82.14%, respectively, compared to that at 1.40 g/cm³, and the saturated water content θs increased by 0.30% and 1.83%, respectively. These results indicated that, in all three soil types, the capacity for water retention diminished with an increase in bulk density, whereas the availability of water within the soil tended to rise as bulk density increases. There were notable variations in the parameters associated with soil water retention capacity across the three types of soil. Under a bulk density of 1.30 g/cm³, the residual moisture content θr of yellow loam and black clay loam increased by 8.07% and 5.25%, respectively, compared to that of yellow sandy loam, while the saturated water content θs increased by 8.83% and 4.88%, respectively. Under the bulk density of 1.35 g/cm³, the θr of yellow loam and Dark loessial soil increased by 6.31% and 5.22%, respectively, compared to yellow sandy loam, while the θs increased by 4.63% and 2.75%, respectively. Under the bulk density of 1.40 g/cm³, the θr of yellow loam and black clay loam increased by 3.45% and 3.34%, respectively, compared to yellow sandy loam, and the θs increased by 2.17% and 1.98%, respectively. These findings indicated that, among the three soils, yellow loam exhibited the best water retention capacity followed by black clay loam with yellow sandy loam having the poorest retention capacity. In terms of water availability, yellow loam was less effective than black clay loam, while yellow sandy loam had better water availability than black clay loam.

Soil porosity

The correlation between volumetric water content and equivalent pore diameter across

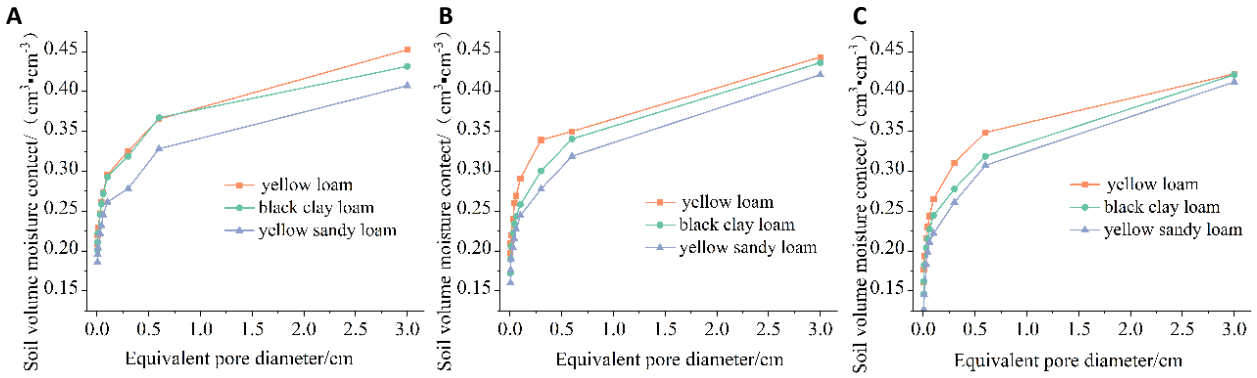

Figure 3. Relationship between equivalent pore diameter and water content under different soil bulk density. **A.** bulk density 1.30g/cm³. **B.** bulk density 1.35g/cm³. **C.** bulk density 1.40 g/cm³.

Table 2. Three kinds of soil porosity under different soil bulk density.

Soil bulk density (g/cm³)	Soil type	Total porosity (%)	Proportion of capillary pores and storage pores (%)
1.30	Yellow - hemp soil	45.74	29.52
	Dark loessial soil	44.33	29.27
	Loessal soil	42.19	26.13
1.35	Yellow - hemp soil	44.64	29.10
	Dark loessial soil	43.61	25.82
	Loessal soil	42.11	24.45
1.40	Yellow - hemp soil	42.81	26.50
	Dark loessial soil	42.46	24.47
	Loessal soil	41.12	23.81

various soil bulk densities demonstrated that, for equivalent pore diameters (d) larger than 0.1 mm, yellow loam exhibited the highest water content at the same equivalent pore diameter, while yellow sandy loam had the lowest moisture content. The water content of black clay loam was slightly lower than that of yellow loam (Figure 3). The results of calculated pore sizes and their distribution demonstrated that, at a bulk density of 1.30 g/cm³, the total porosity of yellow loam and black clay loam increased by 8.41% and 5.12%, respectively, compared to yellow sandy loam with the proportions of capillary pores and storage pores increasing by 13.01% and 12.03%. At a bulk density of 1.35 g/cm³, the total porosity of yellow loam and black clay loam increased by 6.01% and 3.56%, respectively, compared to yellow sandy loam with the proportions of capillary pores and storage pores increasing by 19.03% and 5.62%. At a bulk density of 1.40 g/cm³, the total porosity of yellow loam and black clay loam exhibited increases of 3.91% and 3.06%, respectively, compared to yellow sandy loam. Additionally, the proportions of capillary pores and storage pores rose by 11.28% and 2.67%, respectively. In yellow loam, the total porosity decreased by 6.41% and 4.10% compared to 1.30 g/cm³ and 1.35 g/cm³, respectively, with the proportions of capillary pores and storage pores decreasing by 10.26% and 8.95%. In black clay loam, the total porosity decreased by 4.26% and 2.64% compared to 1.30 g/cm³ and 1.35 g/cm³ with the proportions of capillary pores and storage pores decreasing by 16.47% and 5.32%. In yellow sandy loam, the total porosity decreased by 2.35% and 2.16% compared to 1.30 g/cm³ and 1.35 g/cm³ with the proportions of capillary pores and storage pores decreasing by 8.86% and 2.60% (Table 2). In general, an increase in soil bulk density was

associated with a reduction in total porosity, as well as a decrease in the proportions of capillary and storage pores.

Infiltration characteristics analysis

(1) Wetting front migration distance

During the infiltration process, the maximum depth to which moisture can penetrate is known as the soil wetting front. This front delineates the boundary of the saturated zone and is indicative of the dynamics of water movement influenced by soil matric potential and gravitational forces. The results showed that, during the initial stages of infiltration, the wetting front increased rapidly with time. However, after a period of sustained infiltration, the rate of increase in the wetting front gradually slowed down and stabilized. There were significant differences in the time required for the wetting front to migrate vertically to the same distance across the three soil conditions. When the wetting front migration distance reached 15 cm, the time required for yellow sandy loam was 66.67% and 42.86% longer than that for yellow loam and black clay loam, respectively (Figure 4).

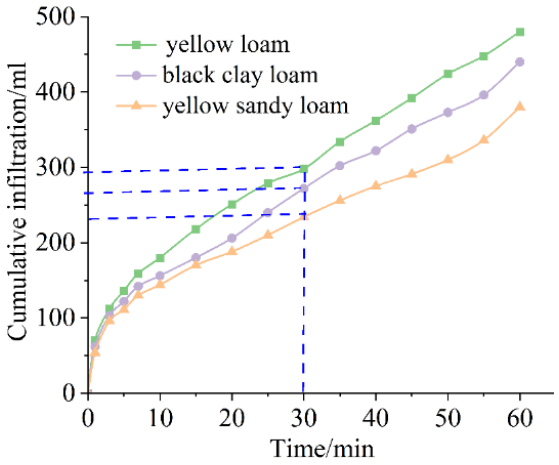

Figure 4. Relationship between vertical migration distance of soil wetting front and time.

To further elucidate the relationship between the wetting front migration distance (*Z*) and time (*t*) under different soil conditions, a fitting analysis was conducted as follows.

$$Z = at^b \quad (5)$$

where the variables a and b were empirical constants. The fitting analysis using a power function for the relationship between the wetting front migration distance and time under different soil conditions demonstrated that the R^2 values were greater than 0.98, indicating a strong power function relationship. The variation range of the parameter among the three soil types was relatively small within 6.42%. In contrast, the exponent *b* gradually decreased with changes in soil type, suggesting that the soil structure had a significant influence on the wetting front migration distance (Table 3).

Table 3. The results of fitting the vertical moving distance and time of soil wetting front under different soil conditions.

Soil type	*a*	*b*	R^2
Yellow - hemp soil	3.2106	0.467	0.9832
Dark loessial soil	3.0169	0.446	0.9863
Loessal soil	3.0606	0.394	0.9932

(2) Cumulative infiltration amount

Cumulative infiltration refers to the total volume of water absorbed per unit area of soil over a given period. This metric is commonly employed to assess the infiltration capacity prior to the attainment of a steady-state infiltration condition. The cumulative infiltration amounts under the three soil conditions exhibited similar trends. During the initial infiltration phase, the cumulative infiltration increased rapidly over time, and after a certain duration, the rate of increase slowed down and approached stability. There were significant differences in the numerical values of cumulative infiltration among the three types of soil. When the infiltration time reached 30 minutes, the cumulative infiltration in yellow sandy loam was 9.56% higher than in black clay loam and 37.35% higher than in yellow loam (Figure 5). To enhance the understanding of the relationship between cumulative infiltration and time across various soil conditions, a fitting analysis was performed utilizing the Kostiakov model to evaluate the

correlation between cumulative infiltration and temporal factors as follows.

$$I = Kt^{\beta} \quad (6)$$

where *I* was cumulative infiltration. *K* and β were defined as empirical constants.

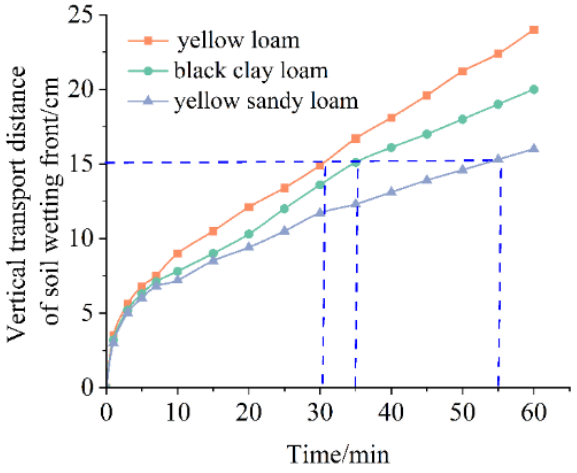

Figure 5. Relationship between cumulative infiltration and time.

When simulating the association between cumulative infiltration and temporal factors across various soil conditions using the Kostiakov model, the R^2 values were all greater than 0.97, indicating a good power function relationship between cumulative infiltration and time across various soil conditions. Both the model coefficient *K* and the exponent β followed the same trend as yellow sandy loam > black clay loam > yellow loam (Table 4). This pattern suggested that soil structure significantly influenced both cumulative infiltration and infiltration rate.

Table 4. The fitting results of cumulative infiltration and time under different soil conditions.

Soil Type	*K*	β	R^2
Yellow - hemp soil	65.253	0.4654	0.9868
Black loessial soil	57.71	0.4648	0.977
Loessal soil	53.905	0.4439	0.9764

Distribution of soil moisture content under different layout methods

Soil moisture content serves as a critical parameter that reflects the hydric condition of the soil. To facilitate data analysis, this study employed the mass moisture content of the soil defined as the ratio of the water content present in the soil to the mass of the dry soil. The spatial distribution of moisture content across the coverage area of the sprinkler combinations for the three soil types under various arrangement methods demonstrated that, within the square configuration, the soil moisture content of the yellow loam exhibited a peak only at position z1 with the highest and the lowest moisture values differing by 5.26%. In the black loess soil, a peak occurred at position z5 with the highest and the lowest moisture values differing by 2.15%. For the yellow sandy loam, the moisture content distribution peaked at the diagonal sprinkler positions z1 and z16 with the highest and the lowest values differing by 2.29% (Figure 6a). The analysis of soil moisture distribution revealed that, within a square arrangement, the yellow sandy loam demonstrated the most uniform distribution of moisture, characterized by relatively minimal overall variations. In contrast, the yellow loam exhibited the highest overall moisture content. Under the equilateral triangular arrangement, the yellow cotton soil exhibited a peak soil moisture content at position t7 with the highest and the lowest values differing by 4.32%. In the black loess soil, the peak moisture content occurred at position t9 with a difference of 4.37% between the highest and the lowest values. The yellow cotton soil had a peak moisture distribution at the same position as that of the black loess soil with the highest and the lowest values differing by 3.59% (Figure 6b). The distribution of soil moisture indicated that, under the equilateral triangular arrangement, the peaks for all three types of soil occurred at similar positions, while the overall distribution of moisture content in yellow cotton soil showed relatively larger variation. Under the rectangular arrangement, the yellow hemp soil exhibited two peaks in soil moisture content at positions j1 and j18 with the highest and the lowest values

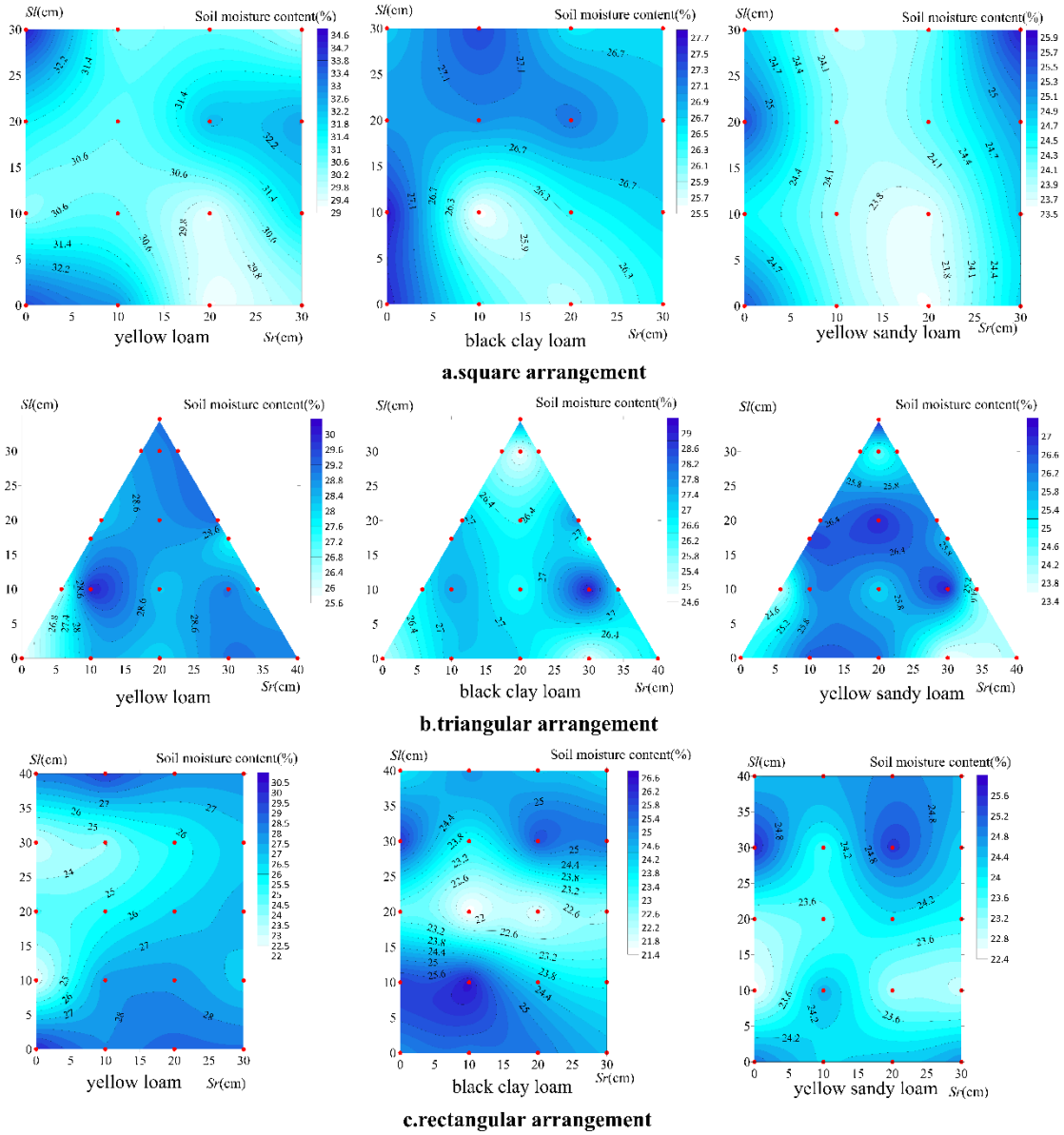

Figure 6. Distribution of moisture water content in different soils under different arrangements.

differing by 7.79%. In the black loess soil, the peak moisture content occurred at position j6 with a difference of 5.12% between the highest and the lowest values. The peak moisture content in yellow cotton soil was found at measurement point j13, where the highest and the lowest values differed by 3.29% (Figure 6c). The analysis of soil moisture distribution revealed that, within the rectangular configuration, the overall moisture distribution in yellow cotton soil was comparatively uniform. In contrast, the moisture content in yellow hemp soil exhibited a higher degree of variability.

Analysis of soil water content distribution uniformity

The soil moisture uniformity coefficient (CUs) described the sum of the absolute deviations of the soil moisture content at each data collection point from the average moisture content within the assessed area, which effectively reflected both the distribution of water and the average

deviation across the entire micro-sprinkler irrigation zone. The CUs values for different soils under various layout conditions showed that, for yellow sandy loam, the triangular layout achieved the highest CUs value, which was 1.53% higher than the square layout and 3.79% higher than the rectangular layout. In black loam, the square layout yielded the highest CUs with increases of 1.52% and 3.19% compared to the triangular and rectangular layouts, respectively. Similarly, for yellow cotton soil, the square layout also achieved the maximum CUs with increases of 0.42% and 1.79% over the rectangular and triangular layouts, respectively (Figure 7).

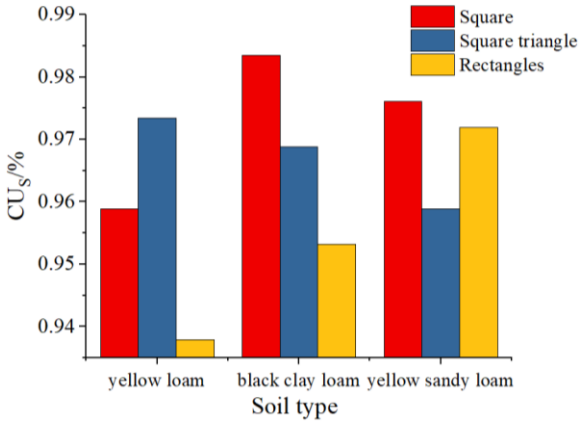

Figure 7. Homogeneity coefficient CUs.

The DUs emphasized the lower portion of soil moisture content at specific measurement points, which was beneficial for ensuring that the minimum soil moisture content reached the levels required by crops. The DUs values for different soils under various layout conditions Showed that the variation trends of DUs across different soil types and layout configurations were generally consistent with those of CUs. Under jute soil conditions, the DUs was the highest for the triangular layout with increases of 0.52% and 6.77% over the square and rectangular layouts, respectively. For both black loam and yellow cotton soils, the square layout showed the highest DUs with increases of 2.57% and 5.77% compared to the rectangular and triangular layouts in black loam and increases of 3.17% and 1.64% in yellow cotton soil, respectively (Figure 8). These results indicated that, for ground-inserted micro-sprinkler irrigation systems, the triangular layout was the optimal arrangement in yellow sandy loam, whereas the rectangular layout performed the least effectively. In contrast, the square layout achieved the best performance in both black clay loam and yellow loam.

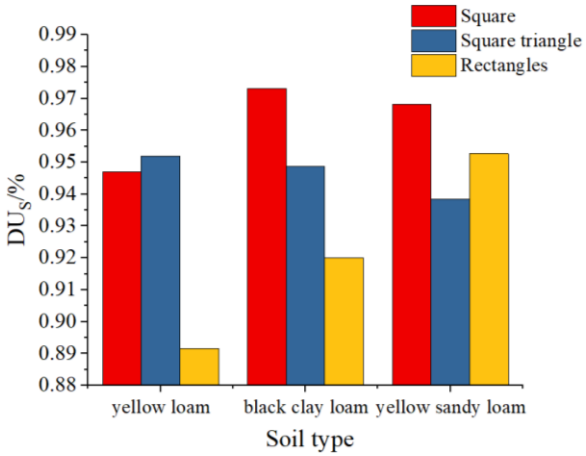

Figure 8. Spread facto DUs.

Discussion

The soil moisture characteristic curve serves as a valuable tool for evaluating the water retention capacity and efficiency of soil moisture across various soil textures. Zheng *et al*. investigated the impact of biochar on soil water retention and discovered that the dimensions, composition, and spatial distribution of soil pores could significantly influence the soil's capacity to retain water [9]. Alnmr *et al*. demonstrated that an increased ratio of large pores to the total pore volume enhanced preferential flow, which in turn led to an elevated rate of water discharge from the soil under identical conditions. This phenomenon consequently diminished the soil's capacity to retain water [10]. Yague *et al*. found that augmenting the capillary porosity of the soil significantly enhanced its water-holding capacity [11], which was influenced by soil texture and structure [12]. The results of this study indicated

that, at lower initial suction, the soil had a larger equivalent pore diameter and greater total porosity, leading to a rapid decline in volumetric water content. As suction increased, the soil began to shrink, leading to an increase in soil bulk density and a reduction in the equivalent pore diameter, characterized by a higher proportion of capillary pores (conduction pores) with the diameter between 0.03 mm and 0.1 mm and storage pores with the diameter less than 0.03 mm until the soil's volumetric water content gradually stabilized. For soils of the same texture but different bulk densities, the porosity decreased with increasing bulk density [13]. Moreover, the capacity for water retention was also affected by its porosity. As bulk density increased, the soil became more compact, resulting in a smaller total porosity and poorer water-holding performance. Similarly, the effectiveness of soil moisture was influenced by the total pore volume and the distribution of soil pores. Soils with lower bulk density tend to have more fine pores between soil particles, resulting in greater capacity for water retention outside the adsorbed water film, thereby enhancing the capacity for water retention of low bulk density soils. The better the capacity for water retention of the soil, the slower the movement of the soil moisture front during infiltration, while the cumulative infiltration amount is greater [14]. In this study, the capacity for water retention of hemp soil was found to be the highest, resulting in the slowest vertical movement speed of the soil moisture front and the largest cumulative infiltration amount, which aligned with the previous findings. Tanaka *et al*. indicated that the highest proportion of small pores in the soil retained water, while the proportion of larger pores used for aeration, drainage, and water conduction was relatively small, which led to a slower moisture movement speed, allowing the soil to retain more water [15]. In contrast, yellow cotton soil exhibited the poorest water-holding capacity with a greater proportion of medium and large pores that had higher capillary suction, resulting in a relatively rapid vertical movement of the soil moisture front compared to hemp soil and black loess, but with less water retention in the soil. Shen *et al*. found that irrigation uniformity significantly affected crop growth and yield on different pressures and lengths of micro-sprinkler tapes for wheat production [16]. Li *et al*. discovered that an appropriate amount of micro-sprinkler irrigation had a significant influence on both crop quality and water use efficiency (WUE) [17]. In this study, under three different soil conditions, there were significant differences in the mean soil moisture content across various layout methods, indicating distinct uniformities in micro-sprinkler irrigation. These uniformities consistently maintained high levels and showed similar trends, suggesting a linear relationship between the soil moisture uniformity coefficient (CUs) and the distribution coefficient (DUs) [18]. This correlation was primarily due to the regulatory effect of moisture migration induced by soil water potential on the distribution of soil moisture, aligning with the findings of Zhang *et al*. [19]. In this study, under the same layout method, the average soil moisture content in hemp soil was the highest, while yellow cotton soil exhibited the lowest, which was consistent with the capacity for water retention of the three soil types. Soils with better water-holding capacity possessed the highest average soil moisture content.

Conclusion

This research analyzed the hydraulic characteristics of the three main cropping soils on the Loess Plateau and proposed the most suitable micro-sprinkler irrigation arrangement in different soils according to their actual water distribution in micro-sprinkler irrigation. The results showed that the soil water characteristic curve was influenced by soil texture and structure. Under the same bulk density conditions, yellow loam exhibited the best water retention performance among the three types of soil, while yellow sandy loam provided the highest soil water availability. For the same type of soil, as the bulk density increased, the capacity for water retention decreased, but the soil water availability improved. The infiltration capacity of

the soil was related to its water retention performance. Among the three main agricultural soils of the Loess Plateau, yellow loam had the slowest wetting front migration distance and the largest cumulative infiltration. Yellow sandy loam showed the fastest wetting front migration distance and the smallest cumulative infiltration. Soils with better water retention performance tended to have slower vertical wetting front movement and higher cumulative infiltration. Under different soil conditions, the layout of micro-sprinklers significantly affected the distribution of soil moisture. Based on the CUs and DUs, the equilateral triangular layout was the optimal arrangement for yellow loam. For black clay loam and yellow sandy loam, the square layout achieved the most uniform soil moisture distribution.

Acknowledgements

This work was supported by the National Natural Science Foundation of China (Grant No. 52469011), the Water Science and Technology Project of Jinan City (Grant No. JNSWKJ202206).

References

1. Kishore P, Chand S, Srivastava SK. 2022. Potential area of micro irrigation and its outreach across Indian states. Indian J Agric Sci. 92(9):1056-1060.
2. Yamauchi T, Pedersen O, Nakazono M, Tsutsumi N. 2021. Key root traits of *Poaceae* for adaptation to soil water gradients. New Phytol. 229(6):3133-3140.
3. Mushayi MM, Kusangaya S, Mujere N. 2023. Use of remote sensing to determine rainwater harvesting sites for piped micro-irrigation schemes in Chimanimani District, Zimbabwe. Water SA. 49(1):56-63.
4. Selva Ganapathi R, Shanthasheela M. 2024. A systematic literature review on adoption and impact of micro-irrigation. J Water Clim Chang. 15(8):4035-4053.
5. Wang CY, Mao XM, Zhao B. 2010. Experiments and simulation on infiltration into layered soil column with sand interlayer under ponding condition. Transactions of the CSAE. 26(11):61-67.
6. Bandala MG, Rovelo COR, Bautista-Capetillo C, González-Trinidad J, Júnez-Ferreira HE, Palestina MS, *et al*. 2022. Analysis of irrigation performance of a solid-set sprinkler irrigation system at different experimental conditions. Water. 14(17):2641.
7. Methods for evaluating irrigation system (Agricultural Handbook No. 82). Edited by Criddle WD. Washington, D.C: U.S. Department of Agriculture. 1956:1-24.
8. Dong QG, Han JC, Zhang Y, Li N, Lei N, Sun ZH, *et al*. 2019. Water infiltration of covering soils with different textures and bulk densities in gravel mulched areas. Appl Ecol Environ Res. 17(6):14039-14052.
9. Zheng J, Li YC, Wang Y, Shi C, Bao TT. 2023. Effects of biochar addition on the infiltration, water and salt distribution of soil irrigated with brackish water. Sci Soil Water Conserv. 21(6):13-22.
10. Alnmr A, Alzawi MO, Ray R, Abdullah S, Ibraheem J. 2024. Experimental investigation of the soil-water characteristic curves (SWCC) of expansive soil: Effects of sand content, initial saturation, and initial dry unit weight. Water. 16(5):627.
11. Yagüe MR, Domingo-Olivé F, Bosch-Serra ÀD, Poch RM, Boixadera J. 2016. Dairy cattle manure effects on soil quality: Porosity, earthworms, aggregates and soil organic carbon fractions. Land Degrad Dev. 27(7):1753-1762.
12. Asadzadeh S, de Souza Filho CR. 2024. A thermal infrared remote sensing approach for estimating soil porosity. Remote Sens Lett. 15(4):384-388.
13. Li Z, Wu PT, Feng H, Zhao XN, Huang J, Zhuang WH. 2009. Simulated experiment on effect of soil bulk density on soil infiltration capacity. Transactions of the CSAE. 25(6):40-45.
14. Dialameh B, Ebrahimian H, Parsinejad M. 2022. Field evaluation of an explicit infiltration function for conventional and alternate furrow irrigation. Irrig Drain. 71(4):1180-1194.
15. Tanaka RT, Weber OL, Torres GN, Miranda JG, Couto EG. 2025. Soil aggregation and organic carbon under different management systems in the Cerrado of Mato Grosso. Revista Caatinga. 38:e12508.
16. Shen XJ, Liu JM, Liu L, Zeleke K, Yi RC, Zhang XP, *et al*. 2024. Effects of irrigation and nitrogen topdressing on water and nitrogen use efficiency for winter wheat with micro-sprinkling hose irrigation in North China. Agr Water Manage. 302:109005.
17. Li ZW, Liu HL, Wang KK, Yao CS, Wang ZM, Zhang YH, *et al*. 2025. Micro-sprinkling irrigation and topsoil compaction improve seedling quality of winter wheat in the Huaibei Plain of China. Plant Soil. 507:967-984.
18. Jiang Y, Wang ZX, Li H, Wang LS. 2024. Optimising the hydraulic performance of a jet impingement sprinkler by varying elevation angle: A comparative study with a non-impingement sprinkler. Biosyst Eng. 245:24-35.
19. Zhang R, Liu YC, Zhu DL, Wu PT, Zhang XM. 2024. Simulating coefficient of soil moisture content uniformity of sprinkler irrigation systems using a COMSOL-3D model. Agr Water Manage. 305:109116.